CrossMark

Hydrothermal controllable synthesis to convert ZnO hexagonal nanotubes to hexagonal nanorods and their photocatalytic application

Raad S. Sabry[1] · M. A. Abid[1] · Baida Muhsen[1] · Wisam. J. Aziz[1]

Abstract Zinc oxide (ZnO) thick films were analyzed by high-resolution X-ray diffraction (HR-XRD), field emission scanning electron microscopy, and photoluminescence (PL) spectroscopy at room temperature. The films were grown on glass substrates using different molar concentrations of aqueous solution (0.02, 0.04, and 0.06 M) via a simple hydrothermal method. This method uses glass bottles with rubber caps as reactor vessels (100 mL) and, thus, is classified as a green chemistry technique. Hexahedral zinc nitrate (Zn $(NO_3)_2 \cdot 6H_2O$), hexamethylenetetramine ($C_6H_{12}N_4$), and deionized water were used as starting materials and were reacted in the presence of heat. HR-XRD measurements confirmed that the diffraction peaks of the polycrystalline structure films can be assigned to the hexagonal-shaped wurtzite ZnO. In addition, the PL spectra show that the integrated intensity decreases with the increase in ZnO content. The SEM images also revealed the existence of hexagonal ZnO nanotubes in the 0.02 M sample, and these nanotubes are gradually converted into hexagonal nanorods with the increase in ZnO content. Moreover, the photocatalytic activity of both nanostructures was measured based on the degradation of methyl blue (MB) by using ultraviolet light ($\lambda = 366$ nm). Results showed that the ZnO nanotubes degraded MB more effectively than the nanorods.

✉ M. A. Abid
  muslim_abid@yahoo.com

  Raad S. Sabry
  raadphy_dr@yahoo.com

  Baida Muhsen
  baida_222@yahoo.com

[1] Physics Department, College of Sciences, Al-Mustansiriya University, Baghdad, Iraq

1 Introduction

One-dimensional nanomaterials, such as nanorods, nanobelts, and nanotubes, have become the focus of intensive research because of their exceptional applications in the fabrication of nanoscale devices [1]. Zinc oxide (ZnO) nanostructures have been the focus of considerable attention because of their unique properties and various applications, including being used as photocatalysts, photoconductor, gas sensor, chemical sensors, ultraviolet (UV) radiation detector, and optoelectronic devices [2, 3]. Given its large exaction binding energy (60 meV) and wide band gap (3.37 eV) at room temperature, ZnO is transparent in visible light and operates in the UV to blue wavelengths; however, ZnO exhibits a crystal structure and optical properties similar to those of gallium nitride-based compounds [4, 5]. Moreover, given their low cost, nontoxic nature, and high photochemical reactivity, ZnO nanostructures employed as photocatalytic degradation material against environmental pollutants have been the focus of considerable attention [6]. Synthesis of ZnO nanostructures has been intensively investigated recently because of their various shapes, such as wires, tubes, rods, flowers, sheets/flakes, particles, stars, belts, and hexagonal prisms, which are produced using various methods, such as evaporation, chemical vapor deposition, and wet chemical processes, including template-based surfactant-assisted precipitation and hydrothermal and solvothermal methods [7, 8]. Among these methods, the hydrothermal method is one of the most common and promising methods used to synthesize isometric ZnO crystals [9]. This method has several advantages, such as one-step synthesis without involving additional processes (e.g., etching or milling), low level of aggression, high purity, environmental friendliness, low cost, and narrow particle size distribution [10]. Moreover,

the hydrothermal method is classified as a green chemistry technique because of its low-temperature reaction in water and in a sealed environment.

The present work determined the different compositions of the aqueous solution of ZnO by using a simple and low-cost hydrothermal method. In addition, the characterization of ZnO epilayers involved the use of high-resolution X-ray diffraction (HR-XRD) to characterize structural properties, field emission scanning electron microscopy (FE-SEM) to characterize the surface morphology, and photoluminescence (PL) measurements to characterize the optical properties of the samples. The photocatalytic activities of the nanostructures were evaluated at room temperature through methyl blue (MB) degradation. The absorption spectra were also obtained using a UV–Vis spectrophotometer.

2 Experiment

Hexagonal ZnO nanotubes exhibiting different compositions were successfully synthesized using a simple and facile hydrothermal method. The films were grown on glass substrates by using aqueous solutions of hexahedral zinc nitrate [$Zn(NO_3)_2 \cdot 6H_2O$, >99 %; Sharlu, Spain] and hexamethylenetetramine HMT ($C_6H_{12}N_4$, >99 %; Aldrich, Germany). The aqueous solution (0.02, 0.04, and 0.06 M; were prepared by adding a 0.4759, 0.9519 and 1.4279 gm of hexahedral zinc nitrate and 0.2243, 0.4486 and 0.6729 gm of HMT, respectively) were dissolved in 80 mL deionized water and then stirred for 5 min. The aqueous solution was passed into 120 mL glass autoclaves containing a pre-cleaned glass substrate. The autoclave was tightly closed, placed in an oven, and then heated at 90 °C for 4 h. Thereafter, the autoclave was allowed to cool down gradually to room temperature. Finally, white thick films were deposited on the glass substrates. The substrates were dipped in deionized water and then dried in air to remove contaminants from the samples. The preparation processes were repeated several times to obtain extra films to analyze the physical properties of the films. The thickness of the ZnO epilayers is between 0.7–0.75 µm as measured by Filmetrics F20-VIS.

The photocatalytic activity of the ZnO nanostructures was measured based on the degradation of MB dye solution. The powdered sample (80 mg) was ultrasonically dispersed in 200 mL of MB solution with a concentration of 20 mg/L. The mixture was stirred in the dark for 1 h to keep the suspension homogenous and to allow physical adsorption of the dye molecules on the catalyst surface. Finally, the mixture was placed under a UV lamp (30 W, λmax = 366 nm; Camag). Approximately 5 mL of the solution was obtained at different time intervals (0, 10, 20, 30, 40, 50, 60, 70, and 80 min). Each sample obtained was centrifuged at 8000 rpm for 20 min to remove any ZnO precipitate, and their absorption spectra were recorded using a UV–Vis spectrophotometer (UV Optima SP-3000 Plus). The formula used to calculate the percentage of dye degradation is expressed as follows:

$$Degradation = ((Co - C)/Co) \times 100\,\%,$$

where Co is the initial dye concentration and C is the dye concentration at time t.

The prepared thick films were examined by XRD (Miniflex II Rigaku, Japan) (Cu Kα) radiation ($\lambda = 1.54178$ Å). The samples were measured in continuous scan mode at a scanning range of 20°–60° and at a scanning speed of 5°/min. The peaks and relative intensities of the XRD patterns were compared with the values from the Joint Committee on Powder Diffraction Standards (JCPDS) card for ZnO (JCPDS 036-1451). Moreover, FE-SEM was used to examine the surface morphology and to estimate the obtained structure uniformity on the substrate. FE-SEM (Hitachi S-4160) is normally operated at 20 kV. The PL measurements are obtained using the Horiba Jobin–Yvon HR-800 UV PL system. He–Cd laser with 325 nm was used as an excitation source. The PL spectra were obtained at room temperature at 330–650 nm.

3 Results and discussion

HR-XRD analyses were conducted to investigate the crystalline quality of the ZnO thick films at room temperature. Figure 1 shows the XRD 2θ scans of ZnO films fabricated on glass substrate with peaks in the (100), (002), and (110) directions by using an aqueous solution technique. The spectra revealed major peaks at 34.37°,
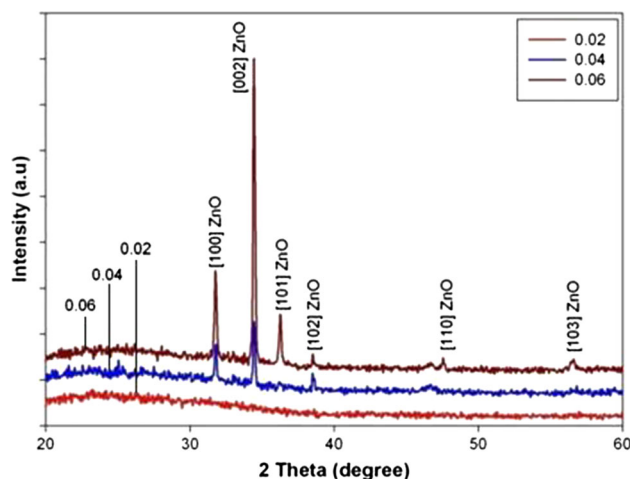

Fig. 1 The XRD pattern of the ZnO thick films with different composition 0.02, 0.04 and 0.06 M

corresponding to ZnO (002). In addition, the (002) crystal orientation of the ZnO films significantly preferred the *c*-axis (002) orientation, which is more intensive than the (100) and (101) crystal orientations. The peaks between 31.67° and 38.44° correspond to the ZnO (100) and ZnO (102) planes, respectively. These results confirm that the films exhibiting these diffraction peaks possess a poly-crystalline structure, which can be assigned to the hexagonal-shaped wurtzite ZnO. Moreover, the diffraction peak from the epilayer fabricated from a low molar concentration of ZnO (0.02 M) slightly increased with the increase in ZnO content, indicating that the changes in the ZnO epilayers increase as the molar concentration of the aqueous solution increases to 0.04 and 0.06 M. Eventually, no diffraction peaks from other impurity phases can be detected.

Figure 2 shows a typical FE-SEM micrograph of the ZnO nanostructures fabricated on a glass substrate through an aqueous solution technique. At first glance of the scanning electron microscopy (SEM) images of the surface, interesting hexagonal-shaped ZnO nanostructures can be observed; however, when we focused and examined the images closely, hexagonal nanotubes are clearly observed in the concentration of 0.02 M and are gradually converted into hexagonal nanorods as the molar concentration of the aqueous solution increases to 0.04 and 0.06 M.

Figures 2a1, a2 show that hexagonal nanotubes were formed at a low molar concentration of the aqueous solution (0.02 M). This result is consistent with that of Yu et al. [11] who proposed that ZnO nanotubes were formed at a low concentration of precursor molecules during electro deposition. The physics behind this observation is that the oxygen decomposed from the raw material can oxidize the surface of the Zn nanobelts resulting in the formation of a thin ZnO shell on the surface, particularly in the hexagonal basal plane; thus, ZnO has a much higher melting point of
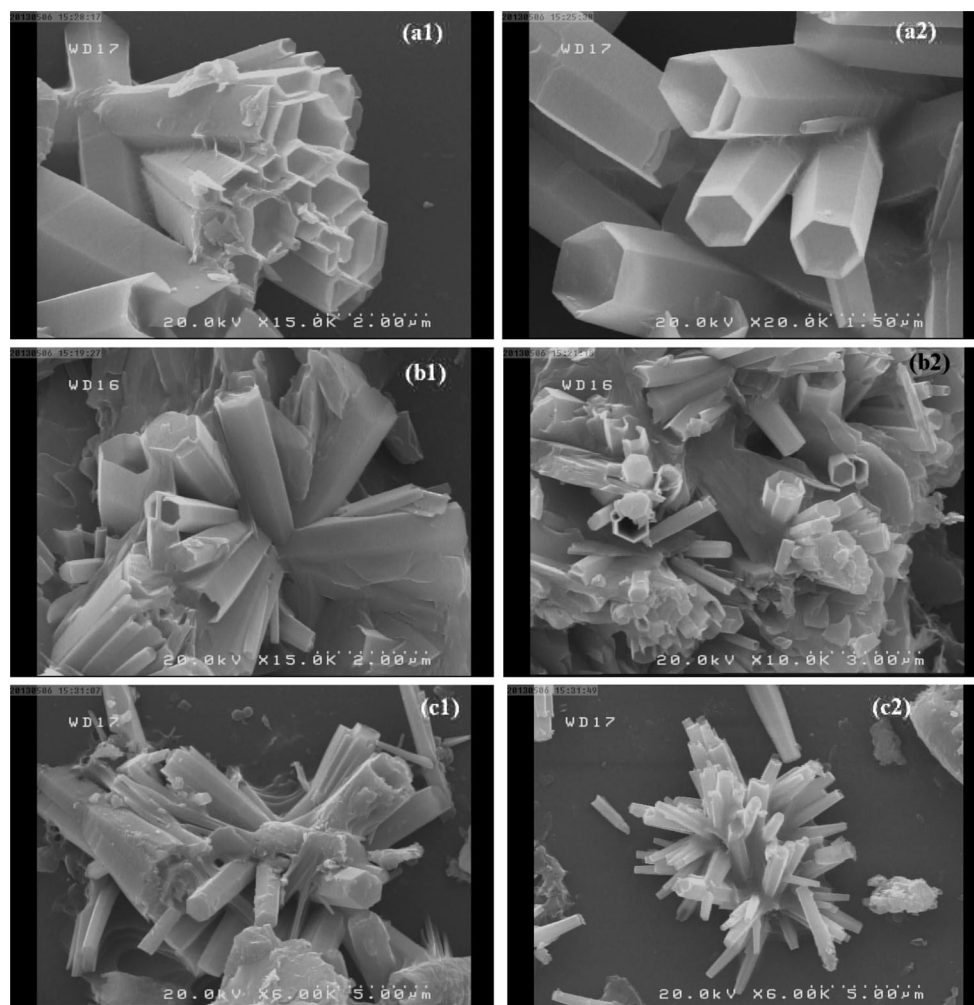

Fig. 2 0.02 M (**a1**, **a2**), 0.04 M (**b1**, **b2**) and 0.06 M (**c1**, **c2**) SEM images of ZnO hexagonal nanotubes, mixture of ZnO hexagonal nanotubes with hexagonal nanorod and ZnO hexagonal nanorod, respectively

1975 °C, than Zn, 419 °C; it is possible for Zn to be sublimated out of the nanobelt at temperatures of 200–300 °C, resulting in the formation of ZnO nanotubes [12]. Li et al. [13] also attributed nanotube formation to the incorporation during the initial growth and the subsequent dissolution of nitrogen-containing organic compounds at the core of ZnO nanowires. In addition, Yang et al. [14] proposed the scrolling of layered structures as the mechanism of nanotube formation. However, the nanotube wall thickness can be precisely controlled by controlling the electro deposition time [15].

Figures 2b1, b2 show that the increase in molar concentration of the aqueous solution from 0.02 to 0.04 M resulted in a mixture of hexagonal nanotubes and nanorods. By contrast, at 0.06 M, the hexagonal nanotubes disappear and are completely converted into hexagonal nanorods (Figs. 2c1, c2. In other words, the nanotube structure that formed at the initial stage of growth will gradually become a nanorod structure as the molar concentration of the aqueous solution increases, indicating that the growth rate become relatively high because of the extremely high degree of saturation of growth nutrients, where the rate of ZnO dissolution is faster than the rate of formation [16].

We obtained the PL spectra of the ZnO samples to provide more direct evidence for the conversion of hexagonal nanotube into hexagonal nanorod. The PL spectrum of ZnO excited by a UV laser at room temperature usually exhibits two emission bands. One band occurs in the UV range and the other band occurs in the visible range; the UV range is attributed to the near-band-edge emission through exciton–exciton collision [17]. By contrast, the visible range is speculated to originate from the electron–hole recombination at a deep-level emission caused by the impurities and structural defects in the crystal (e.g., oxygen vacancies and zinc interstitials) [18].

Figure 3 shows a typical PL spectrum of a ZnO nanostructure at room temperature. The dominant UV emission peak at approximately 358 nm is simultaneously observed with a slightly weak visible emission at 472 nm. A blue shift in the peak position of the near-band-edge exciton emission is possibly caused by the confinement effect [19]. The PL spectra also revealed the decrease in the integrated intensity of the UV range with the increase in ZnO content. This phenomenon is caused by two reasons. First, the ZnO nanotube was completely formed in the initial stage, where the molar concentration of the aqueous solution is 0.02 M. The incident light from the PL laser passes through the nanotubes, causing the photons to bounce back and forth between tube walls and then return back with high intensity (Fig. 4) [20]. Second, ZnO material is preferred as an antireflection coating layer because of its good transparency; therefore, the high refractive index of ZnO ($n = 2.45$) can laterally confine the
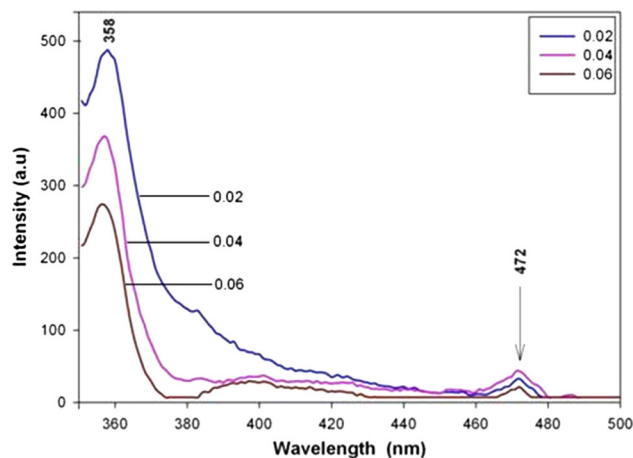

Fig. 3 Room temperature photoluminescence spectrums of 0.02, 0.04 and 0.06 M ZnO nanostructure grown on glass substrates
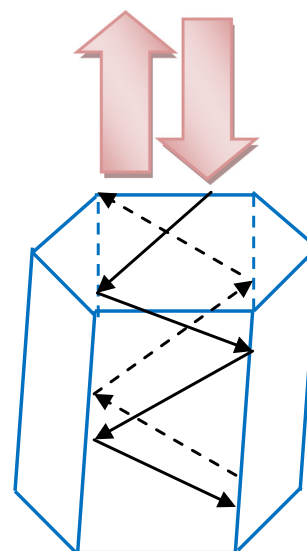

Fig. 4 Schematic illustration of the working principle of a nanotube in which the photons are bouncing back and forth between the tube walls

light traveling inside as a sub-wavelength [20]. However, the low concentration (0.02 M) and the nanotubes that formed prevent ZnO from acting as an antireflection coating layer.

As the concentration increases to 0.04 and 0.06 M, the PL intensity decreases because of the formation of hexagonal nanorod, as shown in the SEM image. In addition, as an antireflection coating layer, ZnO at high concentration enhances light absorption. Lee et al. [21] reported that highly textured ZnO nanorod arrays synthesized through a low-temperature solution growth method can be used as an efficient antireflective coating. The fundamental principle behind this phenomenon is that the complex distribution and the pattern surface of the

nanorods guarantee a gradual reduction of the refractive index from the surface to air and leads to impedance matching between the substrate and air, resulting in photon trapping and reflection suppression over a broad wavelength range [21].

As mentioned previously, the intensity of visible emission in the PL spectra is determined by the concentration of oxygen vacancies in the ZnO samples, and the ratio of the relative intensities of the UV peak to the visible peak indicates the crystallization quality of the samples [i.e., high ratio of UV (visible) peak to visible (UV) peak in the samples indicates high crystallization quality (high defect density)], implying that the ZnO nanostructure samples synthesized under different concentrations exhibit good crystalline quality. The molar concentrations (0.02, 0.04, and 0.06 M) of the ZnO aqueous solution play an important role in the PL emission spectra by ensuring that the optical properties of the ZnO nanotubes and nanorods are sensitive to morphology and defect densities [22].

The photocatalytic activity of the prepared ZnO nanotubes and nanorods was evaluated by MB dye degradation after exposure to UV light. Figure 5 shows the concentration changes in MB dye solution as a function of irradiation time of the photo degradation reactions over ZnO nanotubes and nanorods. The results (Fig. 5) clearly indicate that the synthesized ZnO nanotube photocatalyst exhibits a higher photocatalytic activity than the ZnO nanorods. This difference in photocatalytic activities are attributed to the possible differences in surface area, oxygen vacancies, or polar planes. Before discussing these issues, we must first describe the fundamental mechanism of the photocatalytic reaction that generates electron–hole pairs, as follows: When ZnO nanocatalysts are illuminated by UV light that is stronger than or equal to the band gap energy of ZnO, electro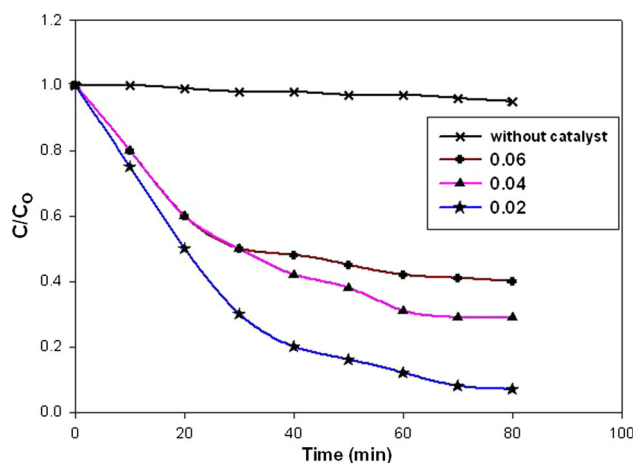ns can be excited from valance band to conduction band and holes are formed in the valance band. These holes and electrons interact with H_2O and O_2, respectively, to yield the OH and OOH hydroxyl radicals; thus, the holes play an important role in photocatalytic reactions. These hydroxyl radicals, which are highly oxidizing in nature, can completely oxidize the dyes by abstracting electron from dye molecules and by breaking the large organic materials into less harmful small organic materials [23, 24].

Then, we focus on the high specific surface area, which exerted a significant effect on photocatalytic activity during the degradation of dyes. One-dimensional nanostructures, such as nanotubes or nanorods, have higher aspect ratio than nanoparticles. When the photocatalyst reached the nanoscale size, the chance of recombining electron–hole pairs decreases because of the fast arrival of electrons at the reaction sites located on the surface of the catalyst [25].

Several studies reported that higher surface area of catalysts did not result in higher catalytic performance [22, 26]. The oxygen vacancies, which are responsible for the green emission in the ZnO nanostructures, promote photocatalytic activity because oxygen vacancies are mainly located at the surface and can serve as electron-capturing center [27, 28]. However, the intensity of visible emission in the PL spectra exhibits a low density of oxygen defect-related vacancies in our samples.

After eliminating the surface areas and oxygen vacancies, only the polar planes, which are the most importing factors affecting photocatalytic activity, are left. Wurtzite ZnO is a classic polar crystal. Two types of wurtzite ZnO (0001) surface structures exist, namely, Zn-polar surfaces with O-atom terminations and O-polar surfaces with Zn-atom terminations; these two polar surfaces exhibit different properties [29].

The morphological models of ZnO hexagonal rods reveal the top surface of O-$(000\bar{1})$ terminations and the bottom surface of Zn-(0001) terminations (Fig. 6a). However, as the rod is converted into a tube, the top and bottom surfaces nearly disappear, although the $(10\bar{1}0)$ surfaces remain intact (Fig. 6b) [22].

Kislov et al. [23] reported that ZnO $(10\bar{1}0)$ surfaces exhibit the highest photocatalytic activity, whereas ZnO

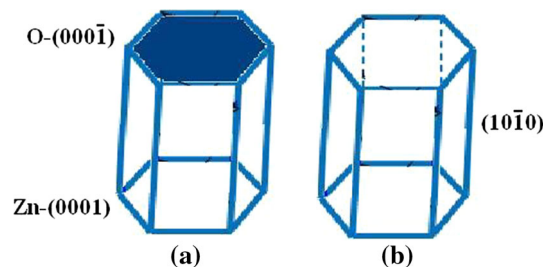Fig. 5 Concentration changes of MB dyes as a function of irradiation time

Fig. 6 The morphology models of ZnO **a** rod and **b** tube

crystals consisting of O-$(000\bar{1})$ and Zn-(0001) termination surfaces show the lowest photocatalytic activity. We can conclude on the basis of the previously presented explanation that the ZnO nanotubes exhibit better photocatalytic activity than nanorods, and this finding is consistent with that of other researchers.

4 Conclusions

Hexagonal ZnO nanostructures were successfully synthesized from aqueous solution containing different molar concentrations (0.02, 0.04, and 0.06 M) of ZnO via a simple and facile hydrothermal method. The XRD results show that the ZnO nanostructure exhibits a wurtzite structure that has a good crystal quality. In addition, the SEM result revealed the existence of nanotubes formed from the low molar concentration of ZnO in the initial stage of growth; these nanotubes are gradually converted into nanorods with the increase in the molar concentration of ZnO. In addition, the PL measurements revealed a reduction in the optical integrated intensity resulting from the existence of nanorods with high concentration of ZnO, which enhances its light absorption capacity as an antireflection coating layer. Moreover, the photocatalytic activity results showed that nanotubes and nanorods have an effect on the degradation of MB compared with that when no catalyst was used. The results showed that ZnO nanotubes degrade MB more effectively than nanorods probably because of the polar planes of tubular structures and the hollow nature of nanotubes, whose ends are both open.

References

1. O. Lupana, G.A. Emelchenko, V.V. Ursaki, G. Chaia, A.N. Redkin, A.N. Gruzintsev, Synthesis and characterization of ZnO nanowires for nanosensor applications. Mater. Res. Bull. **45**, 1026–1032 (2010)
2. O. Lupana, L. Chowb, S. Shishiyanu, E. Monaico, T. Shishiyanua, V. Sontea, B.R. Cuenya, A. Naitabdib, S. Park, A. Schulte, Nanostructure zinc oxide films synthesized by successive chemical solution deposition for gas sensor applications. Mater. Res. Bull. **44**, 63–69 (2009)
3. G.Y. Chaia, L. Chow, O. Lupana, E. Rusu, G.I. Stratan, H. Heinrich, V.V. Ursakie, I.M. Tiginyanu, Fabrication and characterization of an individual ZnO microwire-based UV photodetector. Solid State Sci. **13**, 1205–1210 (2011)
4. L. Chow, O. Lupan, G. Chai, FIB fabrication of ZnO nanotetrapodand cross-sensor. Phys. Status Solidi B **247**(7), 1628–1632 (2010)
5. O. Lupan, L. Chow, G. Chaic, B. Roldana, A. Naitabdia, A. Schulte, H. Heinrich, Nanofabrication and characterization of ZnO nanorod arrays and branched microrods by aqueous solution route and rapid thermal processing. Mater. Sci. Eng. B **145**, 57–66 (2007)
6. C. Wang, X. Wang, B.Q. Xua, J. Zhao, B. Mai, P. Peng, G. Sheng, J. Fu, J. Photochem. Photobiol. **168**, 47 (2004)
7. O. Lupan, G. Chaic, L. Chow, G.A. Emelchenko, H. Heinrich, V.V. Ursaki, A.N. Gruzintsev, I.M. Tiginyanu, A.N. Redkin, Ultraviolet photoconductive sensorbased on single ZnO nanowire applica. Phys Status Solidi A (2010). doi:10.1002/pssa.200983706-&gt
8. C.S. Hsiao, C.H. Peng, S.Y. Chen, S.C. Liou, Tunable growth of ZnO nanorods synthesized in aqueous solutions at low temperatures. J. Vac. Sci. Technol. B **24**, 288–291 (2006)
9. Lv Yu-zhen, C.R. Li, L. Guo, F.C. Wang, Y. Xu, X.F. Chu, Triethylamine gas sensor based on ZnO nanorods prepared by a simple solution route. Sens. Actuators B **141**, 85–88 (2009)
10. Q. Qi, T. Zhang, L. Li, X. Zheng, Q. Yu, Y. Zeng, H. Yang, Selective acetone sensor based on dumbbell-like ZnO with rapid response and recovery. Sens. Actuators B **134**, 166–170 (2008)
11. L. Yu, G. Zhang, S. Li, Z. Xi, D. Guo, Fabrication of arrays of zinc oxide nanorods and nanotubes in aqueous solution under an external voltage. J. Cryst. Growth **299**, 184–188 (2007)
12. Z.L. Wang, J. Phys. Cond. Matter **16**, R829 (2004)
13. Q. Li, V. Kumar, Y. Li, H. Zhang, T.J. Marks, R.P. Chang, Fabrication of ZnO nanorods and nanotubes in aqueous solutions. Chem. Mater. **17**, 1001–1006 (2005)
14. A. Yang, Z. Cui, ZnO layer and tubular structures synthesized by a simple chemical solution route. Mater. Lett. **60**, 2403–2405 (2006)
15. J. Elias, R. Tena-Zaera, G.Y. Wang, C. Levy-Clement, Conversion of ZnO nanowires into nanotubes with tailored dimensions. Chem. Mater. **20**, 6633–6637 (2008)
16. H. Jiang, J. Hu, F. Gu, C. Li, Self-assembly of solid or tubular ZnO rods into twinning microprisms via a hydrothermal route. J. Alloys Compd. **478**, 550–553 (2009)
17. S.C. Lyu, Y. Zhang, H. Ruh, H.J. Lee, H.W. Shim, E.K. Suh, C.J. Lee, Low temperature growth and photoluminescence of well-aligned zinc oxide nanowires. Chem. Phys. Lett. **363**, 134–138 (2002)
18. K.H. Tam, C.K. Cheung, Y.H. Leung, A.B. Djurisic, C.C. Ling, C.D. Beling, S. Fung, W.M. Kwok, W.K. Chan, D.L. Phillips, L. Ding, W.K. Ge, Defects in ZnO nanorods prepared by a hydrothermal method. J. Phys. Chem. B **110**, 20865–20871 (2006)
19. G.W. Ho, A.S.W. Wang, One step solution synthesis towards ultra-thin and uniform single-crystalline ZnO nanowires. Appl. Phys. A **86**, 457–462 (2007)
20. S. Xu, Z.L. Wang, one-dimensional zno nanostructures: solution growth and functional properties. Nano Res. **4**(11), 1013 (2011)
21. Y.J. Lee, D.S. Ruby, D.W. Peters, B.B. McKenzie, J.W.P. Hsu, ZnO nanostructures as efficient antireflection layers in solar cells. Nano Lett. **8**, 1501–1505 (2008)
22. D. Chu, Y. Masuda, T. Ohji, K. Kato, Langmuir **26**(4), 2811–2815 (2010)
23. N. Kislov, J. Lahiri, H. Verma, D.Y. Goswami, E. Stefanakos, M. Batzill, Langmuir **25**, 3310 (2009)
24. S. Baruah, M. Jaisai, R. Imani, M.M. Nazhad, J. Dutta, Sci. Technol. Adv. Mater. **11**, 7 (2010)
25. H.B. Lu, H. Li, L. Liao, Y. Tian, M. Shuai, J.C. Li, M.F. Hu, Q. Fu, B.P. Zhu, Nanotechnology **19**, 045605 (2008)
26. G.R. Li, T. Hu, G.L. Pan, T.Y. Yan, X.P. Gao, H.Y. Zhu, J. Phys. Chem. C **112**(31), 11859–11864 (2008)
27. D. Li, Y.H. Leung, A.B. Djurisic, Z.T. Liu, M.H. Xei, S.L. Shi, S.J. Xu, W.K. Chan, Appl. Phys. Lett. **85**, 1601 (2004)
28. D.S. Bohle, C.J. Spina, J. Am. Chem. Soc. **129**, 12380–12381 (2007)
29. O. Dulub, U. Diehold, G. Kresse, Phys. Rev. Lett. **90**, 016102 (2003)